

# Vibrational dephasing time imaging by time-resolved broadband coherent anti-Stokes Raman scattering microscopy

Young Jong Lee<sup>a)</sup> and Marcus T. Cicerone<sup>b)</sup>

Polymers Division, National Institute of Standards and Technology, Gaithersburg, Maryland 20899, USA

(Received 7 December 2007; accepted 9 January 2008; published online 30 January 2008)

Time delay control in broadband coherent anti-Stokes Raman scattering (CARS) allows acquisition of time-resolved CARS images free of nonresonant background (NRB). We demonstrate that, in some cases, CARS image contrast is not chemical contrast but simply due to differences in NRB. Time-resolved CARS is used to rectify this by eliminating the NRB. We also construct a vibrational dephasing time image from a sequence of time-resolved CARS images of polystyrene beads in toluene. In doing so, we demonstrate the potential of imaging local molecular interactions between molecules and their surrounding in a structured medium. © 2008 American Institute of Physics. [DOI: 10.1063/1.2838750]

Resonant enhancement of coherent anti-Stokes Raman scattering (CARS) provides the intrinsic vibrational contrast mechanism for CARS microscopy. However, the resonant CARS signal is accompanied by coherent nonresonant background (NRB) from the electronic contribution of the solute and solvent. The NRB can pose a significant interference to the signal of interest and often obscures the resonant signal by its associated shot noise. The NRB in broadband CARS is particularly difficult to characterize, making elimination by data fitting difficult and experimental NRB suppression the route of choice.<sup>1,2</sup> Several experimental approaches have been established for reducing or accounting for the NRB contribution. These include polarization control,<sup>3</sup> epi-detection,<sup>4</sup> interference,<sup>2,5</sup> and time-resolved<sup>6</sup> CARS techniques. In general, however, suppression of the nonresonant contribution accompanies resonant signal reduction by more than an order of magnitude.

In particular, time-resolved CARS techniques accomplish NRB suppression by delaying the probe pulse until after the impulsive NRB has decayed. For microscopic imaging, however, time delay cannot be controlled in a two-color scheme, where the pump and probe pulses are degenerate ( $\omega_{\text{pump}} = \omega_{\text{probe}}$ ). Alternatively, a three-color scheme has been used for time-resolved CARS to suppress NRB completely, improving the signal-to-background ratio of a single-frequency CARS image.<sup>6</sup> Recently, a similar three-color scheme has been coupled with multiplex CARS techniques to achieve NRB-free CARS spectra with a high spectra resolution and a broad frequency range simultaneously.<sup>7,8</sup> However, these three-color approaches require three pulses, which have required elaborate laser systems, including kilohertz repetition rate amplifiers and additional optical parametric amplifiers. Recently, time-resolved CARS spectra in a simple two-pulse broadband CARS arrangement has been demonstrated,<sup>9,10</sup> allowing for NRB-suppressed CARS microscopy.

The time-resolved broadband CARS is based on the two-pulse three-color scheme (Fig. 1), where two different frequency components in the continuum pulse (pump/Stokes) populate vibrationally excited states and the subsequent nar-

rowband pulse (probe) induces anti-Stokes Raman emission.<sup>11</sup> The experimental setup of the two-pulse time-resolved broadband CARS is similar to our previous arrangement.<sup>2,11,12</sup> Briefly, as shown in Fig. 1(b), the output (150 fs, centered at 767 nm) of a Ti:sapphire laser oscillator was split into two parts. One part was introduced into a photonic crystal fiber (Femtowhite, Crystal Fibre)<sup>13</sup> to generate a continuum, which was passed through an 850 nm long pass filter. The spectrum of the remaining oscillator output was narrowed to 1.5 nm bandpass filter. The continuum and narrowband beams were introduced colinearly and with parallel polarization into an objective lens. The generated CARS signal was analyzed using a charge-coupled device spectrometer (PhotonMax, Roper Scientific).

Several time-resolved CARS spectra of liquid benzonitrile are shown in Fig. 2(a) at various time delays,  $\Delta t$ . At  $\Delta t < 0$ , when the narrowband (probe) pulse precedes the continuum (pump/Stokes) pulse, the CARS signal is negligible over the whole frequency range. At  $\Delta t = 0$ , when the two pulses arrive simultaneously, the total CARS intensity is maximized and dispersive CARS peaks appear in both higher and lower frequency regions on top of the NRB. At  $\Delta t \geq 1.5$  ps, the NRB throughout the spectrum and the dispersive resonant peaks in the higher frequency region disappear. For  $1.5 \text{ ps} \leq \Delta t \leq 7.5 \text{ ps}$ , the resonant peaks in the lower frequency region remain and their line shape becomes symmetric like spontaneous Raman lines. The time-resolved

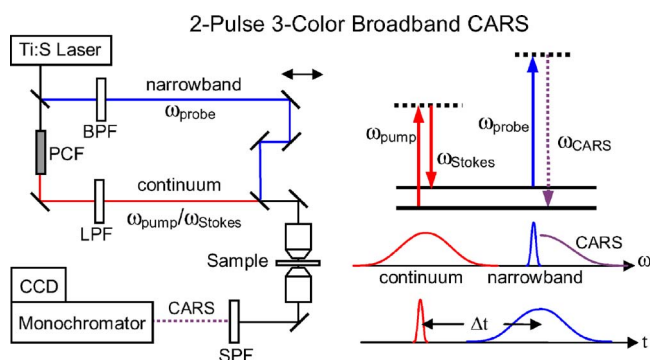


FIG. 1. (Color online) Experimental scheme and energy diagram of two-pulse three-color CARS microscopy setup: BPF, band-pass filter; PCF, photonic crystal fiber; LPF, long-pass filter; and SPF, short-pass filter.

<sup>a)</sup>Electronic mail: yjlee@nist.gov.

<sup>b)</sup>Electronic mail: cicerone@nist.gov.

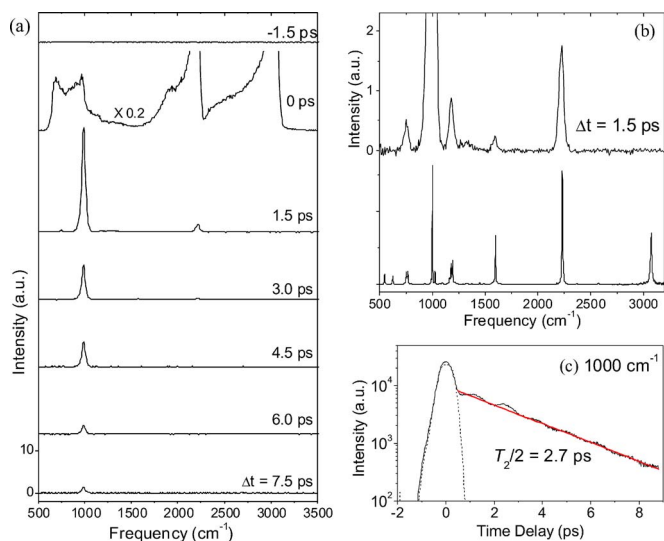


FIG. 2. (Color online) (a) CARS spectra of benzonitrile as a function of the time delay ( $\Delta t$ ). (b) Comparison of the time-resolved CARS spectrum at  $\Delta t=1.5$  ps and a spontaneous Raman spectrum of benzonitrile. (c) Time profile of CARS signal at  $1000\text{ cm}^{-1}$  is fitted to a single exponential decay with a decay time ( $T_2/2$ ) of  $(2.7 \pm 0.1)$  ps, where the uncertainty indicates the standard deviation. The fwhm of the cross correlation (the dashed line) is 800 fs. The powers of the continuum and narrowband pulses are 4.9 and 4.2 mW, respectively.

CARS spectrum at  $\Delta t=1.5$  ps of Fig. 2(a) is enlarged in Fig. 2(b), which reveals NRB-free Raman features, covering the whole fingerprint region ( $<2000\text{ cm}^{-1}$ ). The intensity of the vibrational peak at  $1000\text{ cm}^{-1}$  (phenyl ring mode) decreases at  $\Delta t=1.5$  ps to 30% of that at  $\Delta t=0$  ps and remains detectable even after 7.5 ps. In Fig. 2(c), the intensities at  $1000\text{ cm}^{-1}$  are plotted as a function of  $\Delta t$  and fitted to an exponential decay function  $I(t)=A_0 \exp(-2t/T_2)$  with a time constant of  $T_2/2=(2.7 \pm 0.1)$  ps, where  $T_2$  is the vibrational dephasing time.<sup>14</sup> This measured value agrees with reported values of toluene.<sup>15</sup> In principle, a vibrational dephasing time measured in the time domain corresponds to a linewidth of the equivalent Raman peak in the frequency domain. It is difficult, however, to separate homogeneous line broadening from inhomogeneous line broadening in the frequency domain spectrum. Moreover, a high resolution spectrum often requires a long acquisition time, which makes line shape analysis disadvantageous for imaging applications.

The high repetition rate of the laser and the simplicity of the experimental configuration make the time-resolved broadband CARS technique ideal for imaging, as is demonstrated in Fig. 3. Broadband CARS spectra were measured at  $\Delta t=0$  and 1.5 ps while the sample of  $3\text{ }\mu\text{m}$  polystyrene (PS) beads on a glass coverslip immersed in dimethyl sulfoxide (DMSO) was raster scanned. Figures 3(a) and 3(b) show examples of CARS spectra obtained at  $\Delta t=0$  ps at positions A (PS) and B (DMSO). Contrast for Figs. 3(c) and 3(d) is generated from PS vibration signal at  $\Delta t=0$  and 1.5 ps, respectively. Figures 3(d) and 3(e) are both constructed from the same scanned spectra but contrast is derived from the two different Raman peaks, as indicated in the figure. We note that the DMSO signal of Fig. 3(e) is negligible in the PS beads because they are not swollen by DMSO. In Fig. 3(c), the signal-to-background ratio (S/B) of the image is approximately 2. The contrast for Fig. 3(c) comes primarily from a difference in the level of NRB generated in the two media so

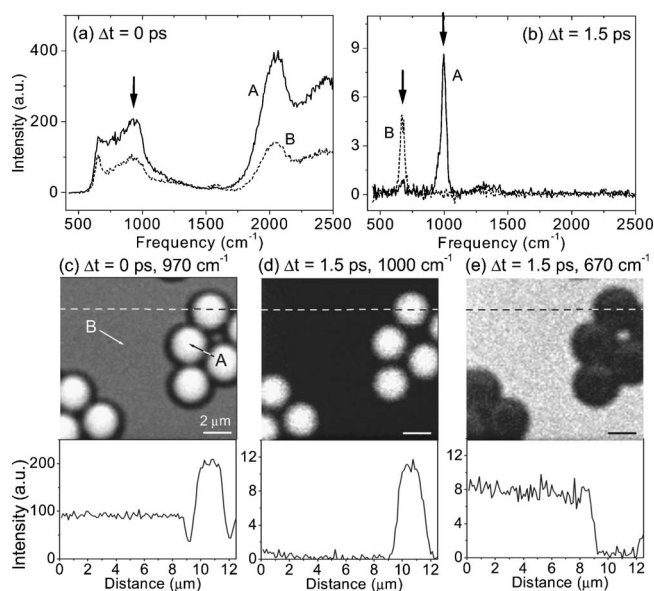


FIG. 3. Broadband CARS images of PS beads in DMSO at  $\Delta t=0$  and 1.5 ps. CARS spectra measured at (a)  $\Delta t=0$  ps and (b)  $\Delta t=1.5$  ps at positions A and B, which correspond to PS and DMSO, respectively. [(c)–(e)] Time-resolved CARS images are constructed at the frequencies corresponding to PS and DMSO modes at different time delays. The powers of the continuum and narrowband pulses are 4.6 and 4.0 mW, respectively. The acquisition time per pixel is 50 ms.

it is fortuitous that there is contrast at all. When the image is acquired at  $\Delta t=1.5$  ps, as in Figs. 3(d) and 3(e), the contrast mechanism has clear chemical origins and an increased signal-to-background ratio ( $S/B > 20$ ). Time-resolved broadband CARS can thus provide “multiplex” Raman imaging data with high chemical specificity in the fingerprint region.

In Fig. 4, we show that CARS images measured as a function of time delay can provide spatially-resolved information on vibrational dephasing times. Figure 4 shows several time-resolved CARS images of PS beads in toluene at different time delays and different frequencies. Figure 4(a) displays spontaneous Raman spectra of PS and toluene. Figure 4(b) displays broadband CARS spectra taken from regions A and B of Fig. 4(e), corresponding to toluene and PS, respectively. It is clear that, due to the similarity of the Raman spectra, the two species cannot be reliably distinguished with the relatively low spectral resolution ( $35\text{ cm}^{-1}$ ) of our broadband CARS microscope. This point is emphasized by comparison of Figs. 4(e) and 4(f). Both of these figures are derived from the same scanned spectra but with contrast coming from a region of a Raman peak [Fig. 4(e)] and a region of no peak [Fig. 4(f)]. As demonstrated by the line scans and visual inspection, there is essentially no difference in the contrast of the two figures; the apparent contrast arises from optical effects at the interface and slight differences in the level of NRB in the two media, similar to Fig. 3(c). The situation is slightly improved for a small positive value of  $\Delta t$ . Figures 4(c) and 4(g) show CARS spectra and a CARS image obtained at  $\Delta t=1.2$  ps. The CARS spectra in Fig. 4(b) are taken from pixels indicated in Fig. 4(g) and represent toluene (A) and PS (B). The line scan below Fig. 4(f) clearly shows enhanced image contrast at this value of  $\Delta t$ . The origin of the contrast, a reduced CARS intensity in PS at this time delay, is due to the shorter vibrational dephasing time of the  $1000\text{ cm}^{-1}$  peak in PS. The vibrational

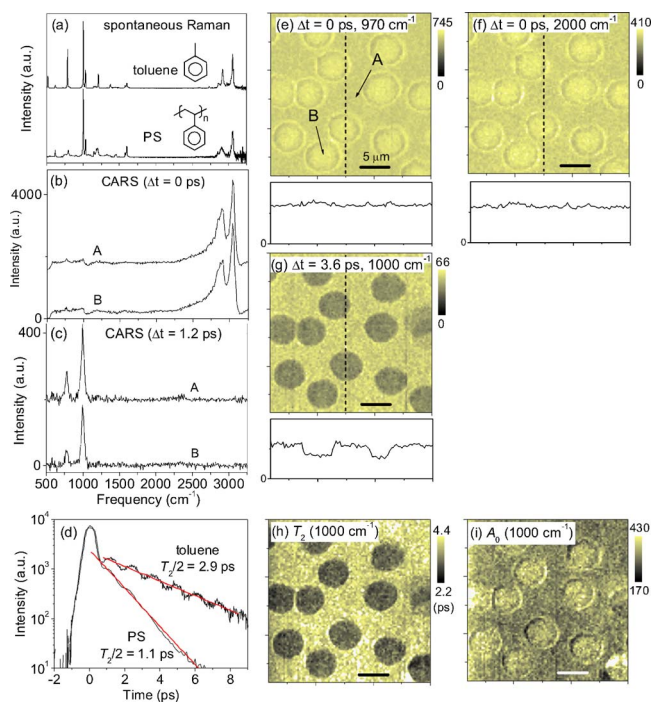


FIG. 4. (Color online) (a) Comparison of spontaneous Raman spectra of neat toluene and a bulk PS plate. [(b)–(c)] Time-resolved CARS spectra at the different positions, A (toluene) and B (PS) at different time delays. (d) Time profiles of  $1000\text{ cm}^{-1}$  Raman mode of neat toluene and the PS plate. CARS images are constructed for (e) resonant ( $1000\text{ cm}^{-1}$ ) and (f) nonresonant ( $2000\text{ cm}^{-1}$ ) frequencies at  $\Delta t = 0\text{ ps}$ . The line scans correspond to the vertical lines in the images. (g) Time-resolved CARS image of the  $1000\text{ cm}^{-1}$  mode at  $\Delta t = 3.6\text{ ps}$ . A series of CARS images measured at  $\Delta t = 1.2, 2.4,$  and  $3.6\text{ ps}$  are fitted to  $I(\Delta t) = A_0 \exp(-2\Delta t/T_2)$  and the dephasing time  $T_2$  and the amplitude  $A_0$  are constructed as (h) and (i), respectively. For the images, the laser powers are 2.0 and 2.7 mW for the continuum and narrowband pulses, respectively. The acquisition time per pixel is 20 ms.

dephasing of the  $1000\text{ cm}^{-1}$  peak in bulk PS and neat toluene is shown in Fig. 4(d).

For a more quantitative analysis, the intensity values  $I(\Delta t)$  of each corresponding pixel in three CARS images, measured at different time delays  $\Delta t$  of 1.2, 2.4, and 3.6 ps, are fitted to  $I(\Delta t) = A_0 \exp(-2\Delta t/T_2)$ . Figure 4(i) shows the image of the amplitude  $A_0$ , which is the NRB-free CARS signal intensity extrapolated to  $\Delta t = 0\text{ ps}$ . Interestingly, the amplitude in PS beads is higher than that in toluene solvent, which indicates either higher phenyl ring density in PS beads or enhanced Raman cross section in a PS matrix. In either case, this type of time independent information cannot be obtained by a single time-resolved CARS image.

Figure 4(h) is the vibrational dephasing time image of the  $1000\text{ cm}^{-1}$  mode constructed by fitting the three CARS images of  $\Delta t = 1.2, 2.4,$  and  $3.6\text{ ps}$ . Vibrational dephasing, ranging typically from several hundreds of femtoseconds to several picoseconds at room temperature,<sup>14,16</sup> is a direct result of an oscillator's vibrational motion being perturbed by interactions with the environment.<sup>15–17</sup> Accordingly, the dephasing mechanisms have been extensively studied as a

means to understand solute-solvent interactions using various methods in the frequency domain (Raman line shape) and in the time domain (time-resolved CARS, photon echo).<sup>16</sup> The dephasing time measurement in the time domain is advantageous for analysis of heterogeneous media since it is independent of inhomogeneous line broadening due to peak position distribution. Unlike conventional time-domain methods that cover only a limited frequency range, the vibrational dephasing time technique that we have demonstrated here can monitor a broad frequency range in a single measurement. This multiplex time-domain technique enables us to measure environmental perturbation that is not reflected in the Raman peak position but only in changes to the vibrational dephasing time, as indicated in the example of Fig. 4(h). The demonstrated method opens up the possibility of characterizing local environments in complex structured media, including polymer blends and biological tissues.

In summary, we have used time-resolved broadband CARS to acquire NRB-free CARS images with high chemical specificity. We have also demonstrated an image of the vibrational dephasing time from a sequence of time-resolved CARS images. The imaging capability of vibrational dephasing times has a potential of observing local molecular interactions in structured materials and cells without introducing labels.

The authors thank the NIH (R21 EB002468-01) for financial support. We also thank Aaron Urbas for measuring the spontaneous Raman spectra. This letter is an official contribution of the National Institute of standards and technology.

- <sup>1</sup>G. I. Petrov and V. V. Yakovlev, *Opt. Express* **13**, 1299 (2005).
- <sup>2</sup>T. W. Kee, H. X. Zhao, and M. T. Cicerone, *Opt. Express* **14**, 3631 (2006).
- <sup>3</sup>J. X. Cheng, L. D. Book, and X. S. Xie, *Opt. Lett.* **26**, 1341 (2001).
- <sup>4</sup>J. X. Cheng, A. Volkmer, L. D. Book, and X. S. Xie, *J. Phys. Chem. B* **105**, 1277 (2001).
- <sup>5</sup>E. O. Potma, C. L. Evans, and X. S. Xie, *Opt. Lett.* **31**, 241 (2006).
- <sup>6</sup>A. Volkmer, L. D. Book, and X. S. Xie, *Appl. Phys. Lett.* **80**, 1505 (2002).
- <sup>7</sup>D. Pestov, R. K. Murawski, G. O. Ariunbold, X. Wang, M. C. Zhi, A. V. Sokolov, V. A. Sautenkov, Y. V. Rostovtsev, A. Dogariu, Y. Huang, and M. O. Scully, *Science* **316**, 265 (2007).
- <sup>8</sup>B. D. Prince, A. Chakraborty, B. M. Prince, and H. U. Stauffer, *J. Chem. Phys.* **125**, 044502 (2006).
- <sup>9</sup>H. Kano and H. Hamaguchi, *J. Raman Spectrosc.* **37**, 411 (2006).
- <sup>10</sup>K. B. Shi, P. Li, and Z. W. Liu, *Appl. Phys. Lett.* **90**, 141116 (2007).
- <sup>11</sup>Y. J. Lee, Y. Liu, and M. T. Cicerone, *Opt. Lett.* **32**, 3370 (2007).
- <sup>12</sup>T. W. Kee and M. T. Cicerone, *Opt. Lett.* **29**, 2701 (2004).
- <sup>13</sup>Certain equipment is identified in this letter to specify adequately the experimental details. Such identification does not imply recommendation by the National Institute of Standards and Technology, nor does it imply that the equipment is necessarily the best available for this purpose.
- <sup>14</sup>H. Hamaguchi and T. L. Gustafson, *Annu. Rev. Phys. Chem.* **45**, 593 (1994).
- <sup>15</sup>H. W. Hubble, T. S. Lai, and M. A. Berg, *J. Chem. Phys.* **114**, 3662 (2001).
- <sup>16</sup>A. Morresi, L. Mariani, M. R. Distefano, and M. G. Giorgini, *J. Raman Spectrosc.* **26**, 179 (1995).
- <sup>17</sup>R. A. Crowell and E. L. Chronister, *J. Phys. Chem.* **96**, 9660 (1992).